Hybrid viscous damper with filtered integral force feedback control

Høgsberg, Jan ; Brodersen, Mark L.

Published in:
Journal of Vibration and Control

Link to article, DOI:
10.1177/1077546314543912

Publication date:
2016

Document Version
Peer reviewed version

Hybrid viscous damper with filtered integral force feedback control

Jan Høgsberg and Mark L. Brodersen

Department of Mechanical Engineering, Technical University of Denmark,
Nils Koppels Allé, building 403, DK-2800 Kongens Lyngby, Denmark

Abstract. In hybrid damper systems active control devices are usually introduced to enhance the performance of otherwise passive dampers. In the present paper a hybrid damper concept is comprised of a passive viscous damper placed in series with an active actuator and a force sensor. The actuator motion is controlled by a filtered integral force feedback strategy, where the main feature is the filter, which is designed to render a damper force that in a phase-plane representation operates in front of the corresponding damper velocity. It is demonstrated that in the specific parameter regime where the damper force leads velocity the control is stable and yields a significant improvement in damping performance compared to the pure viscous damper.

1. Introduction

Supplemental passive dampers (Fu and Kazai, 1998; Sorace and Terenzi, 2008) and base-isolation systems (Snowdon, 1979) are used in many aspects of structural engineering for mitigation of excessive dynamic response (Symans et al., 2008). However, improved damping performance compared to the passive case may be obtained by combining pure energy dissipating installations with active elements to form so-called active/passive or hybrid damper systems (Thenozhi and Yu, 2013). Hybrid systems have been proposed for base-isolation (Beard et al., 1994; Xiong et al., 2000; Shin et al., 2013) and seismic protection systems (Tzan and Pantelides, 1994; Sener and Utku, 1998; Kurata et al., 1999; Kim and Adeli, 2005). In these systems the 'passive' properties of the system are often governed by basic load carrying requirements and thereby appear non-optimal with respect to the transmissibility problem. Thus, the augmentation to hybrid form allows the base-isolation system to maintain its structural integrity, while enhancing the isolation properties by suitable control of the additional active member. Hybrid damper forms have also been suggested in so-called active tuned mass dampers (Lee-Glauser et al., 1997; Mitchell et al., 2012) or active vibration absorbers (Kwak et al., 2002; Tso et al., 2012), where the aim of the active control unit may be to improve the performance of the absorber with respect to transient response during for example an earthquake, reduce the absorber mass without loss of performance or simply increase the operational bandwidth of the absorber. Finally, hybrid control has also been considered in damping layer treatment of beams and plates, where the damping efficiency of passive energy dissipating (constrained) layers is effectively improved by the incorporation of active piezoelectric elements (Benjeddou, 2001; Trindade and Benjeddou, 2002; Trindade, 2011).

In the present paper a pure viscous dash-pot is placed in series with both an active actuator and a force sensor, where the actuator motion is controlled by a decentralized collocated control

algorithm based on feedback from the force sensor. The force feedback concept has been effectively used in space structure applications, where Preumont and coworkers have successfully implemented integral force feedback (IFF) for piezoelectric vibration control of truss structures (Preumont et al., 1992, 2008) and in active tendon control (Preumont and Achkire, 1997). In piezoelectric vibration control the transducer is conveniently placed in series with the force sensor, whereby the force measurement indirectly represents the displacement signal through the elastic properties of the piezoelectric transducer. Thus, the integration of the force provides a signal in phase with the energy conjugated velocity, whereby damping is obtained by IFF. A thorough introduction to the integral force feedback control approach and the corresponding implementation aspects can be found in the book by Preumont (2011). Alternative feedback strategies suitable for especially piezoelectric vibration control have been proposed by Chen and Lurie (1992) and Kanestrøm and Egeland (1995), while Hyde and Anderson (1996) consider the application of force feedback control together with a (viscous) voice coil element instead of a piezoelectric transducer. In the case of active tendon control Guo et al. (2008, 2012) have proposed various modifications of the IFF control by Preumont and Achkire (1997). In Guo et al. (2008) a PI control format is introduced, while recently in Guo et al. (2012) a filtered integral force feedback format results in a stable format which introduces a dissipative viscous component together with a proportional term, representing positive control stiffness. Furthermore, in Smrz et al. (2011) the IFF approach has been modified to give the so-called beta-controller, which is able to effectively introduce damping to the structure and maintain the static stiffness of the active tendons.

The aim of the present paper is to formulate a robust and effective control strategy, where the actuator motion is controlled by a filtered integration of the force feedback signal from the force sensor. Because the actuator is placed in series with the dissipative viscous dash-pot the purpose of the control is to alter the apparent characteristics of the combined device so that larger damping ratios are obtained for the flexible structure, compared to the pure viscous case without active control. The hybrid damper concept is presented in Section 2, which also proposes a calibration of the filter constant. The robustness and performance of the hybrid damper concept are then demonstrated in Section 3, where stability limits are derived in Section 3.1, while the damping efficiency is subsequently assessed in Sections 3.2-3.4 by a root locus, a frequency response and a time transient analysis, respectively. It is shown that for an appropriately filtered force signal the feedback control of the hybrid concept yields a significantly more effective damper system than the passive viscous damper. The results are summarized in Section 4, which also addresses some aspects concerning the possible implementation of the control, and identifies some main limitations and drawbacks of the hybrid viscous damper.

2. The hybrid damper concept

The hybrid damper concept is illustrated in Fig. 1. It is composed of a viscous dash-pot with coefficient c in series with a load cell which measures the damper force $f(t)$ and an active actuator or strut with stroke or piston motion $q(t)$. For structural engineering applications servo-hydraulic

actuators are often used to realize active control strategies, and as demonstrated by Gao and Dyke (2012) the desired actuator motion $q(t)$ may effectively be tracked by a simple PID approach. Furthermore, the experimental setup in Gao and Dyke (2012) combines an actuator placed in series with a load cell and a spring, and it is therefore is similar to the hybrid damper shown in Fig. 1b, which contains a viscous dash-pot instead of an elastic spring.

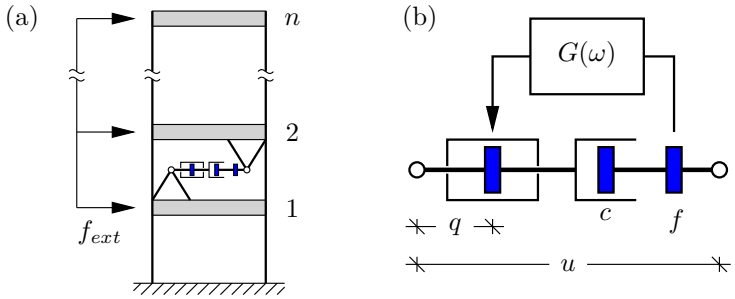

FIGURE 1. (a) Flexible structure with (b) hybrid damper concept.

2.1. **Filtered integral force feedback.** The motion of the hybrid damper is denoted $u(t)$, which means that the velocity over the viscous dash-pot is $\dot{u}(t) - \dot{q}(t)$, where the dot denotes the time derivative. The viscous damper force is therefore given as

$$f(t) \;=\; c\,\big(\dot{u}(t) - \dot{q}(t)\big) \tag{1}$$

The performance of the hybrid damper depends on the particular force feedback control of the actuator motion. In the present paper the actuator velocity $\dot{q}(t)$ is governed by a filtered integral force feedback approach, described by the differential equation

$$\dot{q}(t) \;+\; \tau\ddot{q}(t) \;=\; -g f(t) \tag{2}$$

with control gain g and filter time scale $\tau \geq 0$. For $\tau = 0$ the filter equation (2) recovers the pure integral force feedback (IFF) format introduced by Preumont et al. (1992) for control of piezoelectric transducers, while in the case of a vanishing control gain ($g = 0$) the passive viscous damper without actuator motion ($q = 0$) is recovered.

2.2. **Frequency domain analysis.** The characteristics of the hybrid damper are investigated in the frequency domain by assuming the complex harmonic solution forms

$$u(t) \;=\; \bar{u}\exp(i\omega t) \quad , \quad q(t) \;=\; \bar{q}\exp(i\omega t) \quad , \quad f(t) \;=\; \bar{f}\exp(i\omega t) \tag{3}$$

with angular frequency ω and motion amplitudes identified by a bar. The damper force in (1) is then given as

$$\bar{f} \;=\; i\omega c\,(\bar{u} \,-\, \bar{q}) \tag{4}$$

while the feedback equation (2) can be written as

$$(1 + i\omega\tau)\, i\omega\bar{q} \;=\; -g\bar{f} \tag{5}$$

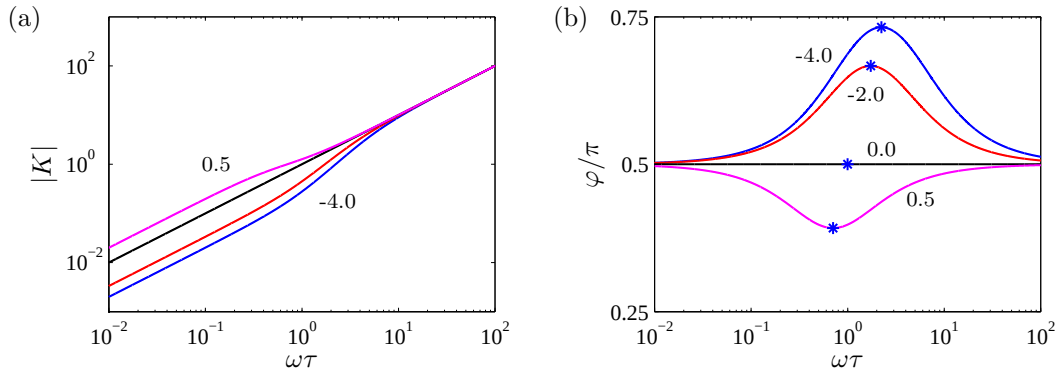

FIGURE 2. (a) Magnitude and (b) phase of the stiffness modulus $K(\omega)$ for $\nu = 0.5$ (magenta), 0.0 (black), -2.0 (red) and -4.0 (blue).

When the actuator stroke q is chosen as the control variable the transfer function

$$G(\omega) \;=\; \frac{-g}{i\omega(1+i\omega\tau)} \tag{6}$$

defines the feedback relation $\bar{q} = G(\omega)\bar{f}$ shown in Fig. 1b.

The damper performance of the hybrid damper is investigated by considering the transfer relation between damper force and damper motion,

$$\frac{\bar{f}}{\bar{u}} \;=\; \frac{c}{\tau}\,\frac{i\omega\tau\,(1+i\omega\tau)}{1-\nu+i\omega\tau} \;=\; \frac{c}{\tau}\,K(\omega) \tag{7}$$

where the non-dimensional control gain is introduced as

$$\nu \;=\; cg \tag{8}$$

The real and imaginary parts of the normalized complex stiffness modulus $K(\omega)$ are

$$\mathrm{Re}[K(\omega)] \;=\; \frac{\nu(\omega\tau)^2}{(1-\nu)^2+(\omega\tau)^2} \qquad , \qquad \mathrm{Im}[K(\omega)] \;=\; \frac{(\omega\tau)\big(1-\nu+(\omega\tau)^2\big)}{(1-\nu)^2+(\omega\tau)^2} \tag{9}$$

The frequency characteristics of the hybrid damper are illustrated in Fig. 2 in terms of the magnitude

$$|K(\omega)| \;=\; \sqrt{\frac{(\omega\tau)^2\big(1+(\omega\tau)^2\big)}{(1-\nu)^2+(\omega\tau)^2}} \tag{10}$$

and the phase angle φ determined from the apparent loss factor relation

$$\tan(\varphi) \;=\; \frac{\mathrm{Im}[K(\omega)]}{\mathrm{Re}[K(\omega)]} \;=\; \frac{1-\nu+(\omega\tau)^2}{\nu(\omega\tau)} \tag{11}$$

Energy dissipation requires that $\mathrm{Im}[K(\omega)] > 0$, which immediately introduces the condition $\nu < 1$. Furthermore, it is seen in Fig. 2b that for $\nu < 0$ the phase angle $\varphi > \frac{1}{2}\pi$. This means that in a phase vector representation, as in Fig. 3a, the damper force f acts ahead of the damper velocity $\dot{u}$. The corresponding time harmonic response is shown in Fig. 3b and it is seen that with a phase lead ($\varphi > \frac{1}{2}\pi$) the force f crosses equilibrium before the velocity $\dot{u}$. As demonstrated in Høgsberg and Krenk (2006) and Høgsberg (2006) such a phase lead of the damper force relative to the velocity results in improved damping performance compared to the pure viscous case with a damper force fully in phase with velocity. In Fig. 2b the control gains $\nu = -2.0$ (red) and -4.0 (blue) represent

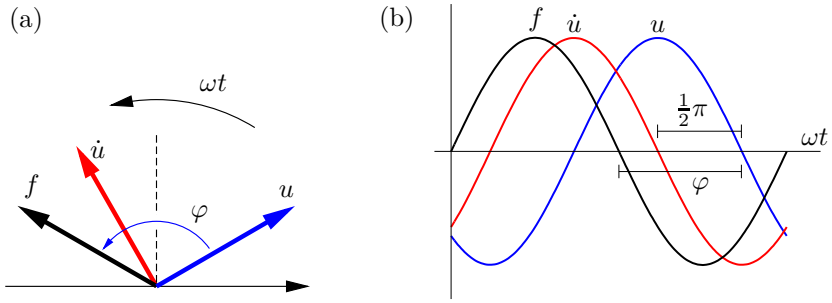

FIGURE 3. (a) Phase-plane vector diagram and (b) response of hybrid damper displacement, velocity and force.

the particular cases with a phase lead, and it is furthermore observed that for negative values of ν the phase angle φ has a maximum with respect to the non-dimensional frequency $\omega\tau$. This is determined by the condition $d\tan(\varphi)/d(\omega\tau) = 0$, which gives the relation

$$\omega\tau \;=\; \sqrt{1-\nu} \tag{12}$$

Substitution of this relation into (11) leads to the reduced expression for the maximum phase angle

$$\tan(\varphi) \;=\; \frac{2\sqrt{1-\nu}}{\nu} \tag{13}$$

In Fig. 2b the solutions comprised of (12) and (13) are marked by asterisks, and the particular case with $\nu = -4.0$ and maximum phase angle $\varphi \simeq 0.75\pi$ is shown in Fig. 3. For the present hybrid concept with $\nu < 0$ the time scale τ should be chosen according to (12) to maximize the phase lead of the damper force and thereby maximize the attainable damping level.

As explained previously equation (2) recovers the IFF control format in the limit $\tau = 0$. It follows from (7) that in this limit the damper force relation reduces to $\bar{f}/\bar{u} = i\omega c/\sqrt{1-\nu}$, and the hybrid damper with pure IFF therefore operates as a viscous damper with viscous coefficient $c/\sqrt{1-\nu}$. In Fig. 2b this property corresponds to all curves approaching the phase angle $\varphi = \frac{1}{2}\pi$ for vanishing non-dimensional frequency ($\omega\tau \to 0$).

3. Damping of a flexible structure

As shown in Fig. 1 it is in the present paper assumed that a single hybrid viscous damper acts on a flexible structure, represented by a discrete numerical model. The equations of motion for the structural degrees of freedom in the vector $\mathbf{u}(t)$ can therefore be written as

$$\mathbf{M}\ddot{\mathbf{u}}(t) \,+\, \mathbf{C}\dot{\mathbf{u}}(t) \,+\, \mathbf{K}\mathbf{u}(t) \;=\; \mathbf{f}(t) \,-\, \mathbf{w}f(t) \tag{14}$$

where $\mathbf{M}$, $\mathbf{C}$ and $\mathbf{K}$ are the mass, damping and stiffness matrix, respectively, $\mathbf{f}(t)$ is the external load vector and $\mathbf{w}$ is the connectivity vector, which defines the spatial attachment of the hybrid damper. The hybrid damper is collocated, which means that the damper motion is $u(t) = \mathbf{w}^T\mathbf{u}(t)$. In Fig. 1 the hybrid damper acts on the relative (horizontal) motion between the first floor and

the second floor of a shear frame type structure, which implies

$$\mathbf{w} \,=\, [\,-1\,,\,1\,,\,0\,,\,\ldots\,,\,0\,]^T$$

In the following the 10 storey version ($n = 10$) of the shear frame structure is used to illustrate the properties and performance of the hybrid viscous damper concept. Details about the shear frame model are provided in Appendix A.

In the remaining part the performance and properties of the hybrid viscous damper are illustrated with respect to damping of flexible structures. It is therefore convenient to eliminate the damper force $f(t)$ in both (14) and (2) by the viscous relation (1), whereby the governing closed-loop equations can be written in compact matrix form,

$$\begin{bmatrix} \mathbf{M} & \mathbf{0} \\ \mathbf{0}^T & \tau \end{bmatrix} \begin{bmatrix} \ddot{\mathbf{u}}(t) \\ \ddot{q}(t) \end{bmatrix} + \begin{bmatrix} \mathbf{C} + c\mathbf{w}\mathbf{w}^T & -c\mathbf{w} \\ \nu\mathbf{w}^T & 1-\nu \end{bmatrix} \begin{bmatrix} \dot{\mathbf{u}}(t) \\ \dot{q}(t) \end{bmatrix} + \begin{bmatrix} \mathbf{K} & \mathbf{0} \\ \mathbf{0}^T & 0 \end{bmatrix} \begin{bmatrix} \mathbf{u}(t) \\ q(t) \end{bmatrix} = \begin{bmatrix} \mathbf{f}(t) \\ 0 \end{bmatrix} \tag{15}$$

with zero column vector $\mathbf{0}$.

Next the stability conditions for the filtered integral force feedback control are derived, whereafter the damping performance is investigated by a root locus, a frequency response and finally a time transient analysis.

3.1. **Closed-loop stability.** The stability of the control is analyzed for the closed-loop system of equations in (15) with external load vector $\mathbf{f}(t) = \mathbf{0}$. These equations are now investigated with respect to Lyapunov stability (Preumont, 2011), for positive and negative values of ν, respectively. The intermediate case with $\nu = 0$ is notoriously stable because it corresponds to passive viscous damping without actuator motion.

3.1.1. *Positive gain.* First consider the case with $g > 0$, whereby $\nu = cg > 0$. With respect to the non-negative energy functional

$$V(\mathbf{u}, \dot{\mathbf{u}}, \dot{q}) \,=\, \frac{1}{2}\dot{\mathbf{u}}(t)^T\mathbf{M}\dot{\mathbf{u}}(t) \,+\, \frac{1}{2}\,\frac{\tau}{g}\,\dot{q}(t)^2 \,+\, \frac{1}{2}\mathbf{u}(t)^T\mathbf{K}\mathbf{u}(t) \,\geq\, 0 \tag{16}$$

the corresponding rate can be obtained from (15) as

$$\dot{V}(\mathbf{u}, \dot{\mathbf{u}}, \dot{q}) \,=\, -\,\dot{\mathbf{u}}(t)^T\mathbf{C}\dot{\mathbf{u}}(t) \,-\, c\left(\dot{u}(t)^2 + \frac{1-\nu}{\nu}\dot{q}(t)^2\right) \tag{17}$$

It is seen that $\dot{V} \leq 0$ for $\nu \leq 1$, whereby the system is Lyapunov stable for $0 < \nu \leq 1$.

3.1.2. *Negative gain.* Now consider the case with $g < 0$, whereby $\nu = cg < 0$. With respect to the non-negative functional

$$V(\mathbf{u}, \dot{\mathbf{u}}, \dot{q}) \,=\, \frac{1}{2}\dot{\mathbf{u}}(t)^T\mathbf{M}\dot{\mathbf{u}}(t) \,-\, \frac{1}{2}\,\frac{\tau}{g}\,\dot{q}(t)^2 \,+\, \frac{1}{2}\mathbf{u}(t)^T\mathbf{K}\mathbf{u}(t) \,\geq\, 0 \tag{18}$$

the corresponding rate can be obtained from (15) as

$$\dot{V}(\mathbf{u}, \dot{\mathbf{u}}, \dot{q}) \,=\, -\,\dot{\mathbf{u}}(t)^T\mathbf{C}\dot{\mathbf{u}}(t) \,-\, c\left(\big(\dot{u}(t) - \dot{q}(t)\big)^2 - \frac{1}{\nu}\dot{q}(t)^2\right) \tag{19}$$

It is found that $\dot{V} \leq 0$ for $\nu < 0$, which means that the system is Lyapunov stable for $\nu < 0$. This concludes the closed-loop stability analysis, which shows that the filtered integral force feedback control is stable for $\nu \leq 1$.

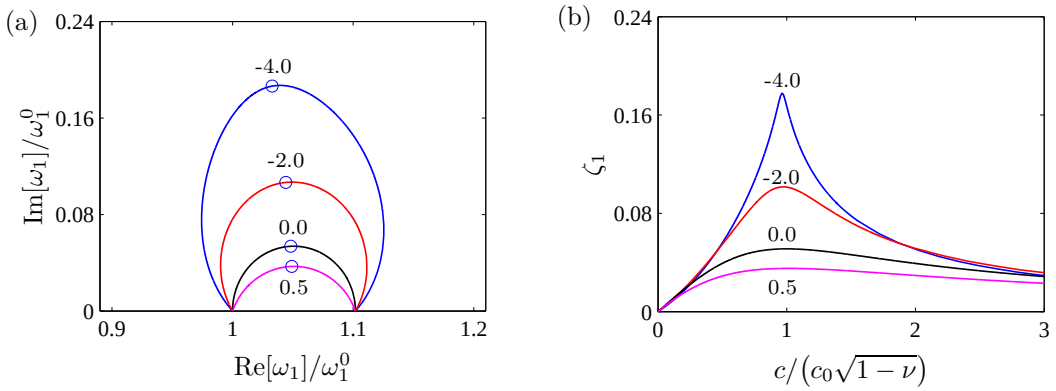

FIGURE 4. (a) Root locus plot and (b) damping ratio for increasing c, with $\nu = 0.5$ (magenta), 0.0 (black), -2.0 (red), -4.0 (blue) and $\tau = \sqrt{1-\nu}/\omega_1^0$.

3.2. **Root locus analysis.** The damping performance of the hybrid damper concept is initially illustrated by a root locus analysis with respect to increasing viscous coefficient c and fixed values of ν and τ. Thus, a particular locus in the complex plane with constant ν the control gain g is inversely proportional to the increasing viscous parameter c via the relation (8). The equations of motion in (15), with external load vector $\mathbf{f}(t) = \mathbf{0}$, are now written in state-space form,

$$\frac{d}{dt}\begin{bmatrix} \mathbf{u}(t) \\ \dot{\mathbf{u}}(t) \\ \dot{q}(t) \end{bmatrix} = \begin{bmatrix} \mathbf{0}\mathbf{0}^T & \mathbf{I} & \mathbf{0} \\ -\mathbf{M}^{-1}\mathbf{K} & -\mathbf{M}^{-1}\left(\mathbf{C} + c\mathbf{w}\mathbf{w}^T\right) & c\mathbf{M}^{-1}\mathbf{w} \\ \mathbf{0}^T & -(\nu/\tau)\mathbf{w}^T & -(1-\nu)/\tau \end{bmatrix} \begin{bmatrix} \mathbf{u}(t) \\ \dot{\mathbf{u}}(t) \\ \dot{q}(t) \end{bmatrix} \tag{20}$$

The complex-valued natural frequencies ω_j associated with damped free vibrations are obtained from the eigenvalues $(i\omega)_j$ of the system matrix in (20). The eigenvalues are in the present analysis directly obtained by the function `damp` in MATLAB. The structural damping matrix $\mathbf{C}$ is omitted in the numerical analyzes of the present paper.

Figure 4a shows the four root loci for the first vibration mode of the 10-storey shear frame structure with $\nu = 0.5$ (magenta), 0.0 (black), -2.0 (red) and -4.0 (blue), respectively. The filter time scale τ is determined according to (12) as $\tau = \sqrt{1-\nu}/\omega_1^0$, where ω_1^0 is the corresponding undamped natural frequency of the first vibration form. Expressions for the natural frequencies and mode shapes of the shear frame model are presented in Appendix A. The curve for $\nu = 0$ in Fig. 4a represents the pure viscous case without piston motion, and details concerning the efficiency and tuning of local viscous dampers on flexible structures are given by Main and Krenk (2005). It is seen in Fig. 4a that improved damping performance is obtained for $\nu < 0$, while the curve for $\nu = 0.5$ indicates that a phase angle $\varphi < \frac{1}{2}\pi$ leads to a reduction in attainable damping compared to the viscous reference case.

Figure 4b shows the corresponding modal damping ratio ζ_1, evaluated as the relative imaginary part of the natural frequency,

$$\zeta_1 = \frac{\mathrm{Im}[\omega_1]}{|\omega_1|} \tag{21}$$

The optimal viscous coefficient is determined with respect to the maximum modal damping ratio for each value of ν by a simple numerical search procedure, and the circles in Fig. 4a represent

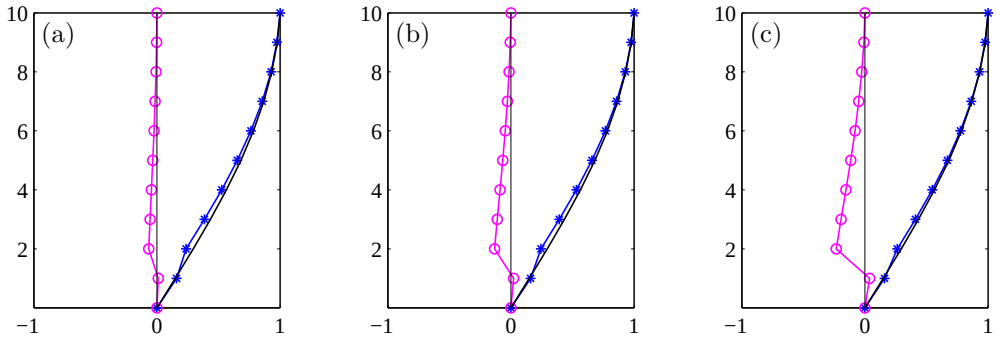

FIGURE 5. Real (blue $*$) and imaginary (magenta $\circ$) part of complex mode shape $\mathbf{u}_1$ for the maximum modal damping case with $\nu = 0$ (a), -2.0 (b) and -4.0 (c).

the complex natural frequencies associated with these optimal viscous coefficients. In Fig. 4b the viscous coefficient c is normalized by the optimal viscous coefficient c_0 for the passive viscous case with $\nu = 0$ and by the correction factor $\sqrt{1-\nu}$. It is seen in Fig. 4b that the normalization of c by $c_0\sqrt{1-\nu}$ estimates the optimal viscous coefficient for the remaining cases ($\nu \neq 0$) with high accuracy. It is furthermore seen from Fig. 4b that the maximum damping ratio $\zeta_{max} = 0.178$ for $\nu = -4.0$ is approximately three times larger than $\zeta_{max} = 0.051$ for the passive case with $\nu = 0.0$, while for $\nu = 0.5$ the maximum damping ratio reduces to $\zeta_{max} = 0.035$. Thus, the proposed filtering of the force signal in (2) leads to a significant increase in attainable damping for $\nu < 0$, compared to the passive viscous case with $\nu = 0$, and in general it may be concluded that attainable damping for the targeted vibration mode increases with decreasing ν.

The complex-valued mode shapes for the first vibration form of the shear frame structure are shown in Fig. 5. The mode shapes are determined for the maximum damping case, represented by the circles in the root locus diagram in Fig. 4a, and normalized to unity at the top floor. The blue curves with asterisks represent the real parts of the mode shape vector, while the magenta curves with circles represent the corresponding imaginary parts. The additional black curves represent the undamped mode shape. Figure 5a shows the passive viscous case with $\nu = 0$, and it is seen that the change in mode shape relative to the undamped case is only moderate. When increasing the magnitude of $\nu < 0$ it is seen in Figs. 5b,c that the imaginary part of the mode shapes increases locally at damper position. This represents a large change in phase angle and thereby a more pronounced wave-like motion of the particular vibration form, which means that the hybrid damper with increasing magnitude of $\nu < 0$ acts increasingly as an energy sink, and consequently dissipates more energy.

3.3. **Frequency response analysis.** The root locus analysis of the previous section represents the idealized case of free vibrations, without any modal interaction. This means that for realistic response and/or loading conditions the attainable damping determined from the root locus analysis may not be entirely realizable. Therefore, forced response characteristics are now considered in terms of a frequency response analysis, where harmonic motion is assumed by the complex

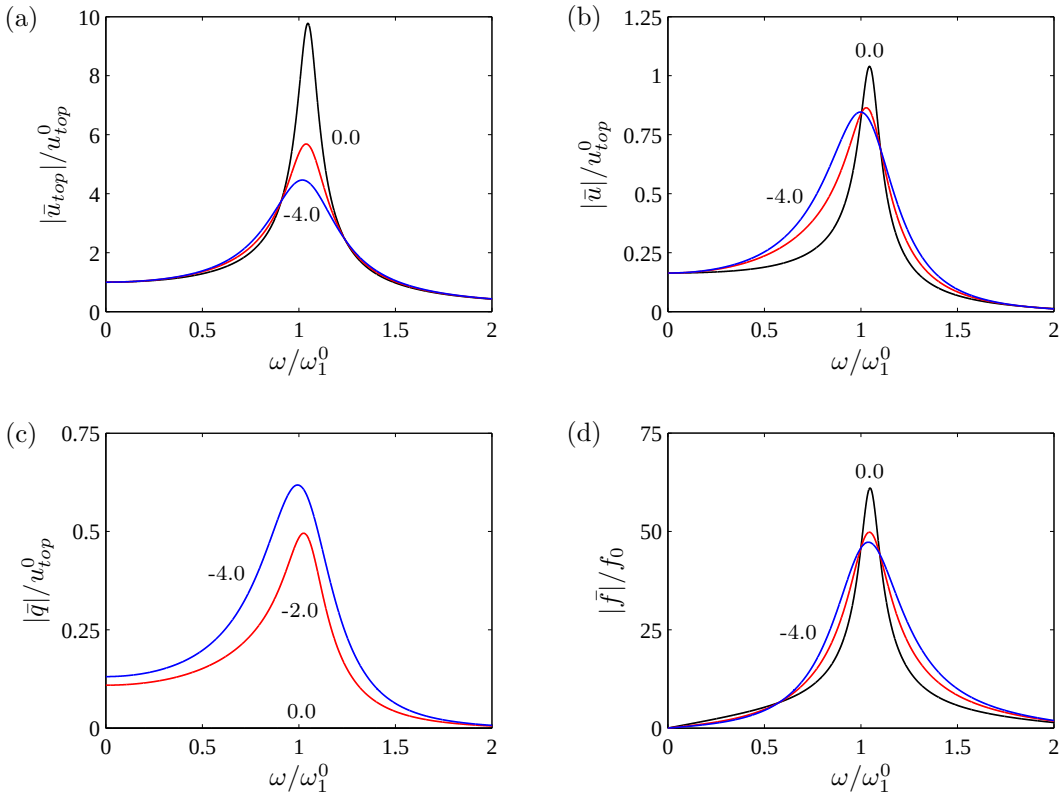

FIGURE 6. (a) Top floor and (b) hybrid damper response and actuator displacement (c) and force (d) with $\nu = 0.0$ (black), -2.0 (red) and -4.0 (blue).

representations

$$\mathbf{u}(t) \,=\, \bar{\mathbf{u}}\exp(i\omega t) \quad , \quad q(t) \,=\, \bar{q}\exp(i\omega t) \quad , \quad \mathbf{f}(t) \,=\, \bar{\mathbf{f}}\exp(i\omega t) \tag{22}$$

where ω represents the driving frequency and a bar denotes the frequency amplitude. Upon substitution of (22) into the governing equations (15), the frequency amplitudes $\bar{\mathbf{u}}$ and $\bar{q}$ can be determined with respect to the load amplitude $\bar{\mathbf{f}}$ from the equation

$$\left(-\omega^2 \begin{bmatrix} \mathbf{M} & \mathbf{0} \\ \mathbf{0}^T & \tau \end{bmatrix} + i\omega \begin{bmatrix} \mathbf{C} + c\mathbf{w}\mathbf{w}^T & -c\,\mathbf{w} \\ \nu\mathbf{w}^T & 1-\nu \end{bmatrix} + \begin{bmatrix} \mathbf{K} & \mathbf{0} \\ \mathbf{0}^T & 0 \end{bmatrix}\right) \begin{bmatrix} \bar{\mathbf{u}} \\ \bar{q} \end{bmatrix} \,=\, \begin{bmatrix} \bar{\mathbf{f}} \\ 0 \end{bmatrix} \tag{23}$$

where the motion of the hybrid damper is subsequently obtained as $\bar{u} = \mathbf{w}^T\bar{\mathbf{u}}$. In the present case the distribution of the external force is assumed to be homogeneous, whereby the force vector can be written as

$$\bar{\mathbf{f}} \,=\, f_0\,[\,1\,,\,1\,,\,\ldots\,,\,1\,,\,1\,]^T$$

with constant load intensity f_0. This homogeneous spatial distribution of the load is chosen because it mainly activates the first vibration mode of the structure and thereby enables a direct comparison with the damper performance found by the root locus analysis in Section 3.2.

Figure 6 shows the frequency dependent amplitudes for the harmonic response of both the structure and the hybrid damper, obtained from (23). The three curves in Fig. 6 represent $\nu = 0.0$ (black), -2.0 (red) and -4.0 (blue), respectively, and the filter time scale is again determined as $\tau =$

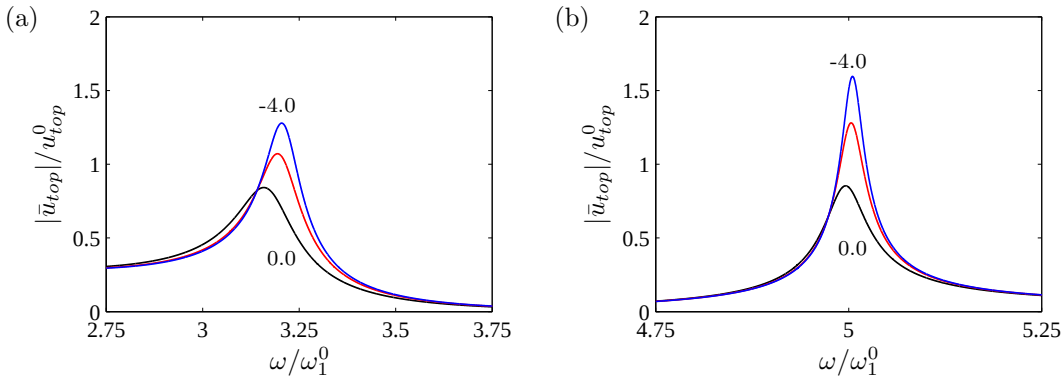

FIGURE 7. Top floor response of (a) second and (b) third vibration modes with $\nu = 0.0$ (black), -2.0 (red) and -4.0 (blue).

$\sqrt{1-\nu}\,/\omega_1^0$. Figure 6a shows the magnitude of the top floor response amplitude $\bar{u}_{top}$ normalized by the corresponding static top floor deflection u^0_{top}, whereby the curves in Fig. 6a represent dynamic amplification factors. It is seen that the amplitude of the structural response is reduced when the magnitude of $\nu < 0$ is increased. At the resonance frequency ($\omega = \omega_1^0$) the dynamic amplification factor is $1/(2\zeta_1)$ when the response is entirely represented by a single mode. In the present case the presence of the damper leads to modal interaction and the estimation of the damping ratio by the resonance peak is therefore only an approximation. From the magnitudes of the resonance peaks in Fig. 6a it is found that $\zeta_1 = 0.051$, 0.088 and 0.112 for $\nu = 0.0$, -2.0 and -4.0, respectively. When comparing these estimates with the results in Fig. 4b it is found that the maximum values obtained by the root locus analysis are not entirely reached, which is due to the significant modal interaction introduced by the hybrid damper, in particular for $\nu < 0$. The amplitude of the hybrid damper stroke $\bar{u}$ is shown in Fig. 6b, and it is seen that $|\bar{u}|$ in fact decreases for increasing magnitude of $\nu < 0$. This is because the phase angle $\varphi > \frac{1}{2}\pi$ for $\nu < 0$, whereby the actuator motion q actively follows the damper force response. And because the magnitude of the actuator motion $|\bar{q}|$, shown in Fig. 6c, increases with the magnitude of ν the total damper motion amplitude $|\bar{u}|$ will consequently decrease. Finally, the damper force amplitude $|\bar{f}|$ is provided in Fig. 6d, which shows that the magnitude of the damper force is also reduced, similar to the damper motion in Fig. 6b. Although the large damping ratios from the root locus analysis are not fully attained, the frequency response analysis demonstrates that the filtered integral force feedback control leads to a significant reduction in the vibration amplitudes for negative values of the non-dimensional control gain ν.

The hybrid damper concept is effective for the targeted vibration mode and the response mitigation improves with increasing magnitude of $\nu < 0$. However, as demonstrated in Fig. 5 increasing the magnitude of ν also introduces a more pronounced change in the vibration mode locally at damper position, which inherently activates higher vibration modes. The consequence of this increasing spill-over is illustrated in Fig. 7, which shows the top floor dynamic amplification for the (a) second and (b) third vibration modes of the shear frame structure. It is seen that when increasing

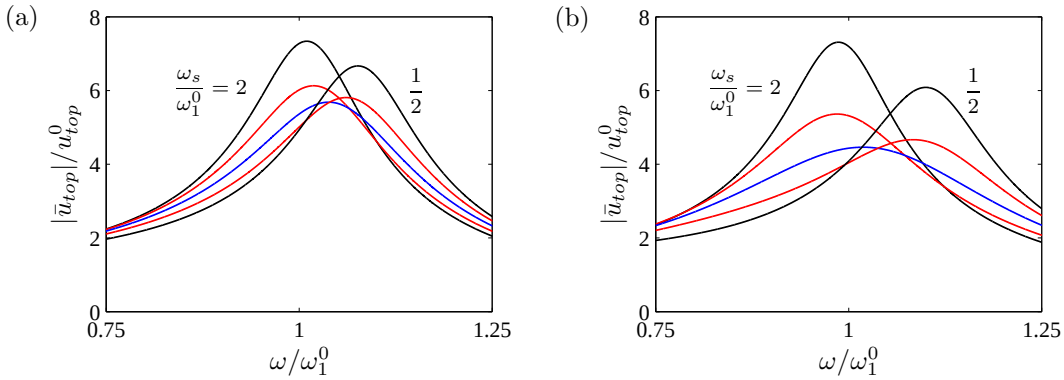

FIGURE 8. Top floor response with (a) $\nu = -2.0$ and (b) -4.0, and $\tau = \sqrt{1-\nu}/\omega_s$ with $\omega_s/\omega_1^0 = 2$ (black), $\frac{4}{3}$ (red), 1 (blue), $\frac{3}{4}$ (red) and $\frac{1}{2}$ (black).

the magnitude of ν the dynamic amplification in fact becomes larger around resonance for these residual modes, which is just opposite the reported behavior in Fig. 6a for the targeted first vibration mode. Thus, a potential disadvantage of using the present hybrid damper concept with negative ν is the more localized damping effort around the target mode compared to the passive viscous damper.

The maximum phase angle of the filtered integral force feedback control is identified by the asterisks in Fig. 2b, and the corresponding time scale is governed by the relation (12) and therefore determined as $\tau = \sqrt{1-\nu}/\omega_s$, where ω_s has been chosen as the natural frequency ω_1^0 of the first vibration mode. Figure 8 shows the dynamic amplification of the top floor response for $\nu = -2.0$ (a) and -4.0 (b), where the five curves, from left to right, in each sub-figure represent $\omega_s/\omega_1^0 = 2$ (black), $\frac{4}{3}$ (red), 1 (blue), $\frac{3}{4}$ (red) and $\frac{1}{2}$ (black), respectively. Thus, the sequence of curves in Fig. 8 illustrates the sensitivity of the control calibration with respect to the change in filter time scale τ. The results in the figure show that $\omega_s = \omega_1^0$ gives the superior amplitude reduction. However, the rather significant detuning of the time scale associated with $\omega_s/\omega_1^0 = \frac{4}{3}$ and $\frac{3}{4}$ also provides good damping performance, and even for the very severe cases $\omega_s/\omega_1^0 = 2$ and $\frac{1}{2}$ the increase in dynamic amplification is limited to around 50%. Thus, the calibration of the filtered integral force feedback control appears to be fairly robust with respect to the choice of filter time scale τ.

3.4. **Time dependent analysis.** This section considers a transient vibration analysis of the shear frame structure in Fig. 1, where the hybrid damper is again located between the first floor and the second floor. The governing system equations are given in (15), and as in the root locus and frequency response analysis structural damping is omitted ($\mathbf{C} = \mathbf{0}$). The governing equations are solved simultaneously by the average acceleration scheme of the Newmark time integration method (Geradin and Rixen, 1997), without introduction of numerical damping. The time increment is chosen so that the vibration period of the first undamped vibration mode is represented by 200 time increments, which implies that the fastest vibration mode of the shear frame structure is sufficiently resolved by approximately 15 time increments.

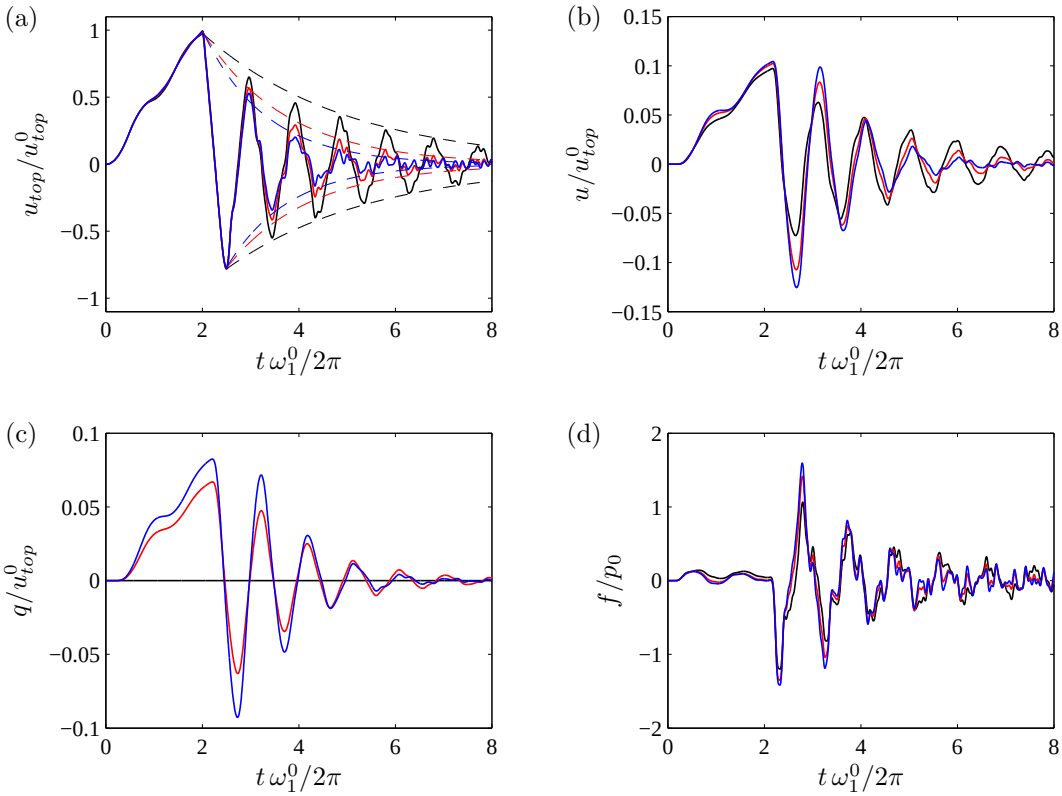

FIGURE 9. (a) Top floor and (b) hybrid damper response, (c) actuator displacement and (d) damper force with $\nu = 0.0$ (black), -2.0 (red) and -4.0 (blue).

In this transient analysis the shear frame structure is loaded locally at the top floor by a linearly increasing force, which is then removed instantaneously after two vibration periods. The time dependent external load vector is given as

$$\mathbf{f}(t) \;=\; p(t)\,[\,0\,,\,0\,,\,\ldots\,,\,0\,,\,1\,]^T$$

where the linear ramping of the load intensity is described as

$$\frac{p(t)}{p_0} \;=\; \begin{cases} t/(2T^0_1) & , \quad t \le 2T^0_1 \\ 0 & , \quad t > 2T^0_1 \end{cases}$$

In this representation $T^0_1 = 2\pi/\omega^0_1$ is the vibration period of the first undamped vibration mode. The local action of the external loading at the top floor together with its transient temporal behavior activate the higher vibration modes of the structure. Thus, the results of this time transient analysis illustrate both the ability of the hybrid viscous damper to damp transient response and the influence of the energy spill-over the from residual modes shown in Fig. 7.

The time histories of the structural and hybrid damper response are shown in Fig. 9, where the three curves in each sub-figure again represent $\nu = 0.0$ (black), -2.0 (red) and -4.0 (blue), and where the filter time scale $\tau = \sqrt{1-\nu}/\omega^0_1$.

The time histories of the top floor response u_{top} are shown in Fig. 9a. The curves are normalized by the corresponding static top floor deflection u^0_{top} associated with the load level p_0. The figure

shows that for $\nu < 0$ the performance of the hybrid damper, assessed in terms of exponential decay, improves with increasing magnitude of ν. The damping ratio ζ_1 is estimated by the logarithmic decrement evaluated between both the first and fourth maximum and the first and fourth minimum of the free vibration response. This procedure gives the average damping ratios $\zeta_1 = 0.053$, 0.093 and 0.124 for $\nu = 0.0$, -2.0 and -4.0, respectively, which are in good agreement with the corresponding estimates from the harmonic analysis of Section 3.3. The exponential decay curves relative to the first maximum and minimum are plotted as dashed curves in Fig. 9a. They are seen to represent the free vibration decay curves fairly well. The significant modal interaction introduced by the filtered force feedback control for $\nu < 0$ results in a quite irregular response at low amplitudes, and in Fig. 9 these irregularities are particularly pronounced due to the omission of structural damping in the present numerical model.

The damper response $u(t)$ is shown in Fig. 9b. For the passive viscous case with $\nu = 0$ the damper motion exhibits a monotonically decaying amplitude envelope. For the active cases with $\nu < 0$ the damper motion experiences an overshoot during the first vibration period of the free response, which counteracts the initial transient response and thereby attenuates the overall vibrations more effectively than the passive viscous damper. Figure 9c shows the actuator motion $q(t)$, which is zero in the passive case with $\nu = 0$, while for $\nu < 0$ the magnitude of the initial transient behavior increases with the magnitude of ν. The damper force $f(t)$ obtained by (1) is finally shown in Fig. 9d. It is seen that the damper force response is quite irregular, with a large initial transient part in the beginning of the free vibration response.

In general, Figs. 9b-d show that the magnitude of the initial transient damper response increases with the magnitude of ν, which is just opposite of what has been concluded for the harmonic analysis in connection with Fig. 6, where the damper amplitudes $\bar{u}$ and $\bar{f}$ are in fact reduced with increasing magnitude of ν. Thus, in the transient analysis the large damper response during the initial part of the free vibration response occurs because the active control of the hybrid damper system is able to compensate the transient structural motion at damper location by a significant actuator motion, which again yields the desired improved response attenuation observed for the top floor response in Fig. 9a.

4. Summary

The hybrid damper is composed of a viscous dash-pot in series with an active actuator and a load cell. A main contribution of the present research is the formulation of a suitably filtered integral force feedback control of the actuator motion, which produces a damper force component that operates ahead of the energy conjugated velocity in a phase-plane vector representation and thereby introduces improved damping performance compared to the passive viscous benchmark damper. The phase lead of the damper force is the key ingredient in the present control format, and as demonstrated in connection with Fig. 2b maximum phase lead is obtained by the relation in (12). Thus, the filter is effectively calibrated by $\tau = \sqrt{1-\nu}/\omega_s$, where ω_s is conveniently chosen as the natural frequency of the particular vibration mode addressed by the hybrid damper. The

time scale in (2) is now eliminated by this relation. Hereby the control equation (2) can be written as

$$\omega_s v(t) + \sqrt{1-\nu}\,\dot{v}(t) = -g\omega_s f(t) \tag{24}$$

where the actuator velocity $v(t) = \dot{q}(t)$ is considered as an independent state variable. The actuator motion $q(t)$ is subsequently found by time integration of the velocity. However, to avoid drift in the actuator motion the integration is conveniently performed via the filter

$$\omega_q q(t) + \dot{q}(t) = v(t) \tag{25}$$

where the first term on the left hand side is introduced to avoid saturation and instabilities in the actuator command signal $q(t)$ by replacing the zero pole $s = 0$ in (2) by the pole $s = -\omega_q$ on the negative real axis in the Laplace domain. This additional term in (25) is similar to the introduction of the 'forgetting factor' in the discrete time realization of the IFF implemented by Preumont et al. (1992). For $\nu = 0$ the feedback control equations (24) and (25) yield $q(t) = 0$ and thereby the passive viscous case, whereas for $\nu < 0$ the actuator motion alters the hybrid damper force so that improved damping performance is obtained with respect to vibration mitigation of flexible structures. However, the application of the hybrid viscous damper is also associated with some limitations and potential drawbacks. First of all the above mentioned saturation and stability issue associated with the integration of the damper force is resolved by adding the first term in (25), which inherently introduces a compromise because the corner frequency ω_q should be chosen small enough not to influence the accuracy and robustness of the integration $v(t) = \dot{q}(t)$, while on the other hand it should be chosen large enough to effectively limit the saturation of the particular actuator. Secondly, it is shown in Fig. 5 that the hybrid damper with a significant magnitude of $\nu < 0$ locally modifies the vibration mode at damper location, which leads to energy spill-over to higher vibration modes resulting in the increased resonant peaks for the residual modes in Fig. 7 and the rather irregular time histories shown in Fig. 9. Finally, Fig. 9 indicates that a main limiting factor of the present hybrid damper concept may be the inherent overshoot of both the damper motion and damper force associated with transient excitation of the flexible structure.

Funding

This work has been supported by The Danish Energy Agency and Vestas Wind Systems A/S under the EUDP project *Monopile cost reduction and demonstration by joint applied research.*

Appendix A. The shear frame structure

The mass and stiffness matrix for the shear frame structure in Fig. 1a are given as

$$\mathbf{M} = m\begin{bmatrix} 1 & & & \\ & 1 & & \\ & & \ddots & \\ & & & 1 \end{bmatrix}, \qquad \mathbf{K} = k\begin{bmatrix} 2 & -1 & & \\ -1 & 2 & & \\ & & \ddots & -1 \\ & & -1 & 1 \end{bmatrix} \tag{A.1}$$

where m is the concentrated floor mass and k represents the apparent stiffness of the connecting walls. As demonstrated in for example Luco et al. (1992) the natural frequencies for this discrete shear frame model are

$$\omega_j^0 \;=\; 2\Omega \sin\left(\frac{\pi}{2}\,\frac{2j-1}{2n+1}\right) \qquad , \qquad j = 1, 2, \ldots, n \tag{A.2}$$

where $\Omega = \sqrt{k/m}$ represents the natural frequency of a single-storey structure. The corresponding components of the undamped mode shape vector $\mathbf{u}_j^0$ are

$$u_{j,k}^0 \;=\; \sin\left(\pi k\,\frac{2j-1}{2n+1}\right) \qquad , \qquad j, k = 1, 2, \ldots, n \tag{A.3}$$

where index k denotes the floor number (degree of freedom). The modal mass and modal stiffness associated with this undamped vibration form are

$$m_j \;=\; \mathbf{u}_j^{0\,T}\mathbf{M}\mathbf{u}_j^0 \qquad , \qquad k_j \;=\; m_j(\omega_j^0)^2 \tag{A.4}$$

For the 10-storey shear frame structure ($n = 10$) it is found that the lowest natural frequency is $\omega_1^0 = 0.1495\Omega$, while the fastest $\omega_n^0 = 1.978\Omega$ is close to 2Ω.

References

Beard AM, Schubert DW and von Flotow AH. (1994) A practical implementation of an active/passive vibration isolation system. *Proceedings of SPIE* 2264: 38-49.

Benjeddou A (2001) Advances in hybrid active-passive vibration and noise control via piezoelectric and viscoelastic constrained layer treatments. *Journal of Vibration and Control* 7: 565-602.

Chen CS and Lurie BJ (1992) Active member bridge feedback control for damping augmentation. *Journal of Guidance, Control, and Dynamics* 15: 1155-1160.

Fu Y and Kazai K (1998) Comparative study of frames using viscoelastic and viscous dampers. *Journal of Structural Engineering* 124: 513-522.

Gao X, Dyke SJ (2014) Modeling and control of actuators for high performance structural dynamic testing. *Smart Materials and Structures* 23: 055008 (8pp).

Geradin M and Rixen D (1997) *Mechanical Vibrations. Theory and Application to Structural Dynamics*, 2nd edition. Wiley, Chichester, UK.

Guo T, Liu Z, Cai L (2012) An improved force feedback control algorithm for active tendons. *Sensors* 12: 11360-11371.

Guo T, Lu Q and Li J (2008) PI force feedback control for large flexible structure vibration with active tendons. *Acta Mechanica Sinica* 24: 721-725.

Høgsberg JR (2006) *Modelling of Dampers and Damping of Structures*. PhD thesis, Technical University of Denmark, Kongens Lyngby, Denmark. ISBN 87-89502-59-0.

Høgsberg JR and Krenk S (2006) Linear control strategies for damping of flexible structures. *Journal of Sound and Vibration* 293: 59-77.

Hyde TT and Anderson EH (1996) Actuator with built-in viscous damping for isolation and structural control. *AIAA Journal* 34: 129-135.

Kanestrøm RK and Egeland O (1995) Maximum power absorption with active struts. *Journal of Guidance, Control, and Dynamics* 18: 907-908.

Kim H and Adeli H (2005) Hybrid control of smart structures using a novel wavelet-based algorithm. *Computer-Aided Civil and Infrastructure Engineering* 20: 7-22.

Kurata N, Kobori T, Takahashi M, Niwa N and Midorikawa H (1999) Actual seismic response controlled building with semi-active damper system. *Earthquake Engineering and Structural Dynamics* 28: 1427-1447.

Kwak MK, Kwak MH and Heo S (2002) Development of the passive-active vibration absorber using piezoelectric actuators. *Proceedings of SPIE* 4697: 292-300.

Lee-Glauser GJ, Ahmadi G and Horta LG (1997) Integrated passive/active vibration absorber for multistory buildings. *Journal of Structural Engineering* 123: 499-504.

Luco JE, Wong HL and Mita S (1992) Active control of the seismic response of structures by combined use of base isolation and absorbing boundaries. *Earthquake Engineering and Structural Dynamics* 21: 525-541.

Main JA and Krenk S (2005) Efficiency and tuning of viscous dampers on discrete systems. *Journal of Sound and Vibration* 286: 97-122.

Mitchell R, Kim Y, El-Khorchi T and Cha YJ (2012) Wavelet-neuro-fuzzy control of hybrid building-active tuned mass damper system under seismic excitations. *Journal of Vibration and Control* 19: 1881-1894.

Preumont A 2011. *Vibration Control of Active Structures. An Introduction*, 3rd edition. Springer, Heidelberg.

Preumont A and Achkire Y (1997) Active damping of structures with guy cables. *Journal of Guidance, Control, and Dynamics* 20: 320-326.

Preumont A, De Marneffe B, Deraemaeker A and Bossens F (2008) The damping of a truss structure with a piezoelectric transducer. *Computers and Structures* 86: 227-239.

Preumont A, Dufour JP and Malékian C. (1992) Active damping by a local force feedback with piezoelectric actuators. *Journal of Guidance, Control, and Dynamics* 15: 390-395.

Sener M and Utku S (1998) Adaptive base isolation system for the control of seismic energy flow into buildings. *Journal of Intelligent Material Systems and Structures* 9: 104-115.

Shin YH, Moon SJ, Kim JM, Cho HY, Choi JY and Cho HW (2013) Design considerations of linear electromagnetic actuator for hybrid-type active mount damper. *IEEE Transactions on Magnetics* 49: 4080-4083.

Smrz M, Bastaits R and Preumont A (2011) Active damping of the camera support mast of a Cherenkov Gamma-ray telescope. *Nuclear Instruments and Methods in Physics Research A* 635: 44-52.

Snowdon JC (1979) Vibration isolation: Use and characterization. *Journal of the Acoustical Society of America* 66: 1245-1274.

Sorace S and Terenzi G (2008) Seismic protection of frame structures by fluid viscous damped braces. *Journal of Structural Engineering* 134: 45-55.

Symans MD, Charney FA, Whittaker AS, Constantinou MC, Kircher CA, Johnson MW and McNamara RJ (2008) Energy dissipation systems for seismic applications: Current practice and recent developments. *Journal of Structural Engineering* 134: 3-21.

Thenozhi S and Yu W (2013) Advances in modeling and vibration control of building structures. *Annual Review in Control* 37: 346-364.

Trindade MA (2011) Experimental analysis of active-passive vibration control using viscoelastic materials and extension and shear piezoelectric actuators. *Journal of Vibration and Control* 17: 917-929.

Trindade MA and Benjeddou A (2002) Hybrid active-passive damping treatments using viscoelastic and piezoelectric materials: Review and assessment. *Journal of Vibration and Control* 8: 699-745.

Tso MH, Yuan J and Wong WO (2012) Suppression of random vibration in flexible structures using a hybrid vibration absorber. *Journal of Sound and Vibration* 331: 974-986.

Tzan SR and Pantelides CP (1994) Hybrid structural control using viscoelastic dampers and active control systems. *Earthquake Engineering and Structural Dynamics* 23: 1369-1388.

Xiong YP, Xing JT, Price WG and Wang XP (2000) Hybrid active and passive control of vibratory power flow in flexible isolation systems. *Shock and Vibration* 7: 139-148.